Hysteresis of contact angle of sessile droplets on smooth homogeneous solid substrates via disjoining/conjoining pressure

I.Kuchin, V.Starov*

Department of Chemical Engineering, Loughborough University, LE11 3TU, UK,
V.M.Starov@lboro.ac.uk

Abstract

A theory of contact angle hysteresis of liquid droplets on smooth, homogeneous solid substrates is developed in terms of shape of disjoining/conjoining pressure isotherm and quasi-equilibrium phenomena. It is shown that all contact angles, θ, in the range $\theta_r < \theta < \theta_a$, which are different from the unique equilibrium contact angle $\theta \neq \theta_e$, correspond to the state of slow "microscopic" advancing or receding motion of the liquid if $\theta_e < \theta < \theta_a$ or $\theta_r < \theta < \theta_e$, respectively. This "microscopic" motion almost abruptly becomes fast "macroscopic" advancing or receding motion after the contact angle reaches the critical values θ_a or θ_r, correspondingly. The values of the static receding, θ_r, and static advancing, θ_a, contact angles in cylindrical capillaries were calculated earlier, based on the shape of disjoining/conjoining pressure isotherm. It is shown now that both advancing and receding contact angles of a droplet on a on smooth, homogeneous solid substrate (i) can be calculated based on shape of disjoining/conjoining pressure isotherm, (ii) both advancing and receding contact angles depend on the drop volume and are not unique characteristics of the liquid-solid system. The latter is different from advancing/receding contact angles in thin capillaries. It is shown also that the receding contact angle is much closer to equilibrium contact angle than the advancing contact angle. The latter conclusion is unexpected and is in a contradiction with commonly accepted view that the advancing contact angle can be taken as the first approximation for the equilibrium contact angle. The dependency of hysteresis contact angles on the drop volume has a direct experimental confirmation.

Key words: droplets, contact angle hysteresis, surface forces

*Corresponding author: V.M.Starov@lboro.ac.uk

Introduction

Earlier a theory of contact angle hysteresis of menisci in thin capillaries has been developed [1,2] based on a s-shape of disjoining/conjoining pressure isotherm. The nature of the disjoining/conjoining pressure can be briefly explained as follows. The properties of liquid in the vicinity of liquid-air and solid-liquid interfaces differ from the corresponding properties in the bulk because of surface forces action. We refer to these layers where the surface forces act, as boundary layers (nothing to do with hydrodynamic boundary layers). In the vicinity of an apparent three phase contact line these boundary layers overlap. This overlapping of boundary layers is the reason why disjoining/conjoining pressure appears.

Contact angle hysteresis on smooth homogeneous substrates appears in the case of partial wetting, when disjoining/conjoining isotherm has a special s-shape. Components contributing to the formation of disjoining/conjoining pressure are discussed in [3-6]. These components are

1) electrostatic component, which is caused by formation of electrical double layers and their overlapping:

$$\Pi_E = RTc_0(\exp(\varphi) + \exp(-\varphi)) - 2RTc_0 - \frac{(RT)^2\varepsilon\varepsilon_0}{2F^2}\left(\frac{\partial\psi}{\partial y}\right)^2, \qquad (1)$$

where R,T, F, ε, ε_0 are universal gas constant, temperature in ^{o}K; Faraday's constant, dielectric constant of water and dielectric constant of vacuum, respectively; c_0 is electrolyte concentration; y and ψ are the co-ordinate normal to the liquid-air interface and dimensionless electric potential in F/RT units, respectively.

The electric potential ψ and the surface charge density σ in Eq.(1) are related as [5]

$\sigma_h = \varepsilon\varepsilon_0 \frac{RT}{F}\left(\frac{\partial\psi}{\partial y}\right)_{y=h}$ for the liquid/vapour interface;

$\sigma_s = -\varepsilon\varepsilon_0 \frac{RT}{F}\left(\frac{\partial\psi}{\partial y}\right)_{y=0}$ for the solid/liquid interface;

2) structural component, which is caused by water molecule dipoles orientation in a vicinity of interfaces and overlapping of these structured layers. This component is presented as a combination of both short-range and long-range interactions [7]:

$$\Pi_S = K_1 \exp(-h/\lambda_1) + K_2 \exp(-h/\lambda_2), \qquad (2)$$

where K_1, K_2 and λ_1, λ_2 are parameters related to the magnitude and the characteristic length of the structural forces. The subscripts 1 and 2 correspond to the short-range and

long-range structural interactions, respectively. Currently the latter four constants can be extracted from experimental data only;

3) molecular or van der Waals component [3,5]:

$$\Pi_M(h) = \frac{A}{6\pi h^3}, \qquad (3)$$

where $A = -A_H$, A_H is the Hamaker constant. Note, the importance of the van der Waals component is usually grossly exaggerated in the literature: other components of the disjoining/conjoining pressure are equally or even more important in the case of aqueous electrolyte solutions.

The resulting disjoining/conjoining pressure isotherm has a characteristic s-shape [5,7]:

$$\Pi(h) = \Pi_M(h) + \Pi_E(h) + \Pi_S(h). \qquad (4)$$

Hysteresis of contact angle on smooth homogeneous substrates

It is usually believed that the static hysteresis of contact angle is determined by the surface roughness and/or heterogeneity. No doubt that a roughness and/or a chemical heterogeneity of the solid substrate contribute substantially to the contact angle hysteresis. In this case it is assumed that at each point of the surface the equilibrium value of the contact angle at that point is established, depending only on the local properties of the substrate. As a result a whole series of local thermodynamic equilibrium states can be realized corresponding to a certain interval of values of the contact angle. The maximum possible value corresponds to the value of the static advancing contact angle, θ_a, and the minimum possible value corresponds to the static receding contact angle, θ_r.

However, the roughness and/or heterogeneity of the surface are apparently not the sole reasons for contact angle hysteresis. Over the last years there have been an increasing number of publications which confirmed the presence of contact angle hysteresis even on smooth, homogeneous surfaces [8-13]. The most convincing evidence for the presence of the above mentioned phenomenon is its presence on free liquid films [14-19]. In the latter case surfaces of free liquid films are not rough at all and are also chemically homogeneous. Hence, in the case of contact angle hysteresis on free liquid

films it is impossible to explain the hysteresis phenomenon by the presence of roughness and/or heterogeneity.

Below we describe a mechanism of contact angle hysteresis based on the consideration of surface forces, which act in the vicinity of the apparent three-phase contact line. This type of contact angle hysteresis is present even on a smooth, homogeneous substrate. Consideration of this kind of contact angle hysteresis on rough and/or non-homogeneous surfaces from this point of view is to be undertaken.

Evidently only a single unique value of equilibrium contact angle, θ_e, is possible on a smooth, homogeneous surface. Hence, the hysteresis contact angles $\theta_a \neq \theta_e$, $\theta_r \neq \theta_e$ and all contact angles in between, which are observed experimentally on such surfaces, correspond only to non-equilibrium states of the system. The discussion of the hysteresis phenomenon below is based on the analysis of non-equilibrium states of the system: droplets on smooth homogeneous solid substrate.

Equilibrium contact angle of sessile droplets and surface forces (disjoining/conjoining pressure)

The equilibrium profile of a sessile two dimensional droplet is described by the following equation [1,2,5]:

$$\frac{\gamma h''}{(1+h'^2)^{3/2}} + \Pi(h) = P_e, \qquad (5)$$

where γ is the liquid-vapour interfacial tension, *h(x)* is an equilibrium droplet profile. The variable *h* and its derivatives *h'* and *h''* are the functions of *x* coordinate. However, in some cases below the variable *x* is excluded and the implicit functions *h'*(*h*) and *h''(h)* are considered.

According to the Kelvin's law

$$P_e = \frac{RT}{v_m}\ln\frac{p_s}{p} = -\frac{\gamma}{R_e}, \qquad (6)$$

where v_m the molar liquid volume; p_s and p are saturated vapour pressure and the pressure of the vapour, which the sessile droplet is at equilibrium with. See Fig.1 for details. As follows from Eq (6), the liquid can be at equilibrium with oversaturated vapour only, that is only if $p>p_s$. It is very difficult to keep oversaturated vapour over sessile droplet over a prolong period of time. This explain why equilibrium sessile droplets is so difficult (if possible at all) to investigate experimentally.

According to Eq. (5) the whole profile of a drop can be subdivided into three parts (Fig. 1): a spherical cap (using this part a *macroscopic* contact angle can be determined), a transition zone, where both capillary pressure and disjoining/conjoining pressure are equally important, and a flat equilibrium liquid film region ahead of the drop.

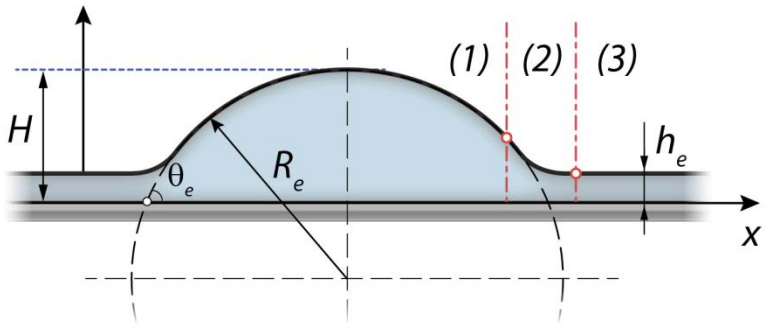

Fig. 1. Equilibrium drop: *(1)* spherical cap, where capillary forces dominate, *(2)* transition zone, where capillary forces and disjoining/conjoining pressure are equally important, and *(3)* flat equilibrium film in front of the drop solely determined by surface forces action.

The second order differential equation (5) can be integrated once, which gives:

$$\frac{1}{\sqrt{1+h'^2}} = \frac{C - P_e h - \int_h^\infty \Pi(h)dh}{\gamma} \quad , \qquad (7)$$

where C is an integration constant to be determined. The integration was made within limits from h to H, but the term $P_e H$ is a constant which was included into the integration constant C. It is assumed in Eq. (7) that the droplet height H>> t_s, where t_s is radius of surface forces action.

Note that there are two boundary conditions, which solution (7) should satisfy (see below) at h=h_e and at h=H. However, there is only one integration constant C in Eq. (7), hence, should be one extra condition on the solutions of Eq. (7) [1, 2]: this extra condition allows to express the contact angle vis disjoining pressure isotherm.

According to the transversality condition $h'(h_e) = 0$ [20], the integration constant in Eq. (7) is $C = \gamma + P_e h_e + \int_{h_e}^\infty \Pi(h)dh$. Hence, the drop profile is described by the following equation:

$$\frac{1}{\sqrt{1+h'^2}} = \frac{\gamma - \varphi(h, P_e)}{\gamma} \qquad (8)$$

where

$$\varphi(h,P_e)=P_e\left(h-h_e\right)-\int_{h_e}^{h}\Pi dh\,. \qquad (9)$$

The left hand side of Eq. (8) should be always positive and less or equal to 1, hence, the following inequality should be satisfied:

$$0\le\varphi(h,P_e)\le\gamma \quad , \qquad (10)$$

where the left part of the inequality corresponds to a zero derivative h', and the right one corresponds to an infinite value of h'.

On the other hand at the drop apex, *H*, the derivative vanishes, $h'(H)=0$. This together with Eq. (7) and assumption H >> t_s results in $C=\gamma+P_eH$. Then Eq. (7) can be rewritten as:

$$\frac{1}{\sqrt{1+h'^2}}=\frac{\gamma+P_e(H-h)-\int_{h}^{\infty}\Pi(h)dh}{\gamma}\,. \qquad (11)$$

Outside the range of the disjoining/conjoining pressure action, that is at h>> t_s, Eq. (11) reduces to

$$\frac{1}{\sqrt{1+\overline{h}'^2}}=\frac{\gamma+P_e(H-\overline{h})}{\gamma}, \qquad (12)$$

which describes the spherical cap of the drop in Fig. 1. The magnitudes $\overline{h}'$ [m/m] and $\overline{h}$ [m] describe the spherical cap profile in the absence of surface forces. Intersection of the latter profile with the solid substrate defines an apparent three-phase contact line and the macroscopic equilibrium contact angle: $\overline{h}'(0)=-\tan\theta_e$. Then Eq. (12) can be rewritten at $\overline{h}=0$ as $P_e=-\frac{\gamma(1-\cos\theta_e)}{H}$. Casting this expression into Eq. (11) results in the following expression for the equilibrium contact angle in the case of drops on a flat substrate:

$$\cos\theta_e=1+\frac{\frac{1}{\gamma}\int_{h_e}^{H}\Pi(h)dh}{1-\frac{h_e}{H}}\approx 1+\frac{1}{\gamma}\int_{h_e}^{\infty}\Pi(h)dh,\quad \text{for}\quad h_e\sim t_s<<H\,, \qquad (13)$$

where $t_s\approx 100$ nm is the radius of surface forces action.

Eq.(13) shows that the equilibrium contact angle θ_e is only a function of the disjoining/conjoining pressure in the region of thicknesses $h_e<h<H$, which corresponds to

the transition region 2 in Fig. 1. This is because the local capillary pressure $\frac{\gamma h''}{(1+h'^2)^{3/2}}$ in Eq.(5) is a supplements of the disjoining/conjoining pressure Π(h) to the constant value P_e, which is fixed at any position *x*. From this point of view, the dependence Π(h) determines the forces acting inside the transition zone and, hence, the form of the liquid profile inside the transition zone as well as the value of the equilibrium contact angle in Eq. (13).
Eq. (13) shows that for the *partial* wetting case the following condition should be satisfied:

$$\int_{h_e}^{\infty} \Pi(h)dh < 0 . \qquad (14)$$

It is possible to show [1,2] that the height of equilibrium sessile drops, *H,* decreases with increasing *over*saturation, when the absolute value of P_e increases. It follows also from Kelvin's equation (6): the small droplets (with low sizes R_e and *H*) are characterized by higher pressure, P_e, and high *over*saturation ratio, p_s/p. A mathematical relation between *H* and P_e can be obtained from Eq.(11) at *h'*=0: $H = h_e + \frac{1}{P_e}\int_{h_e}^{\infty} \Pi dh$.

However, the decrease in *H* has certain limits, since drops can be at the equilibrium with flat films only if $P_e > \Pi_{min}$ (Fig. 2). Curve 2 (Fig. 2) shows Π_{min} is the pressure corresponding to the minimum of the isotherm $\Pi(h)$ in the case of partial wetting. For $P_e < \Pi_{min}$ there is neither a film nor a drop on the solid surface at equilibrium. When P_e decreases and approaches $\Pi_{min,}$ when drops whose size decreases, will be "torn" off the surface and pass into the vapor phase. However, at $0>P_e > \Pi_{min}$ when the equilibrium drops are possible, the equality $P_e = \Pi(h_e)$ implies that the profile curvature corresponding to the first term in Eq.(5) is equal to zero at the state of equilibrium. This is a reason why a drop can be at equilibrium with flat films only.

Note that the equilibrium contact angle defined by Eq. (13) is not completely determined by the shape of the disjoining/conjoining pressure isotherm: it also depends on the lower limit of integration, h_e, which is determined by the equilibrium excess pressure P_e. In other words, the *equilibrium* contact angle of drops depends on the *equilibrium* volume of the drop, which can vary from "infinity" (at $P_e=0$) to a minimum value at $P_e=\Pi_{min}$ (Fig. 2).

Fig. 2 illustrates the dependence of the disjoining/conjoining pressure on the thickness of a flat liquid film for the cases of *complete* wetting (curve 1, which corresponds to $\Pi_M(h)$ typical for oil drops on glass substrates) and *partial* wetting (curve 2, which

corresponds to Eq. (14), typical for drops of aqueous electrolyte solutions on glass substrates).

The dependency 2 (Fig. 2) is usually accepted in the case of partial wetting. However, actually only some parts of this dependency can be experimentally measured: (i) only disjoining/conjoining pressure at thicknesses where the stability condition, $\frac{d\Pi(h)}{dh} < 0$, is satisfied [5], (ii) only disjoining/conjoining pressure at under-saturation, that is, at $P_e>0$ (Fig. 2). This means that disjoining/conjoining pressure can be experimentally measured only at thicknesses below t_0 (*α* films) and above t_{max} (β films)(Fig.2). That is, currently it is impossible to say if there is only one minimum on the dependency 2 (Fig. 2) or there is one extra minimum on this dependency in the region $P_e<0$ at relatively big thicknesses $h> t_{max}$. The presence of such minimum (secondary minimum) is well known in the case of interaction between colloidal particles [5], however, the presence of the secondary minimum in the case of disjoining/conjoining pressure has not been discussed before. It is shown below that there is a reasonable theoretical background for existence of the secondary minimum on dependency 2 (Fig. 2).

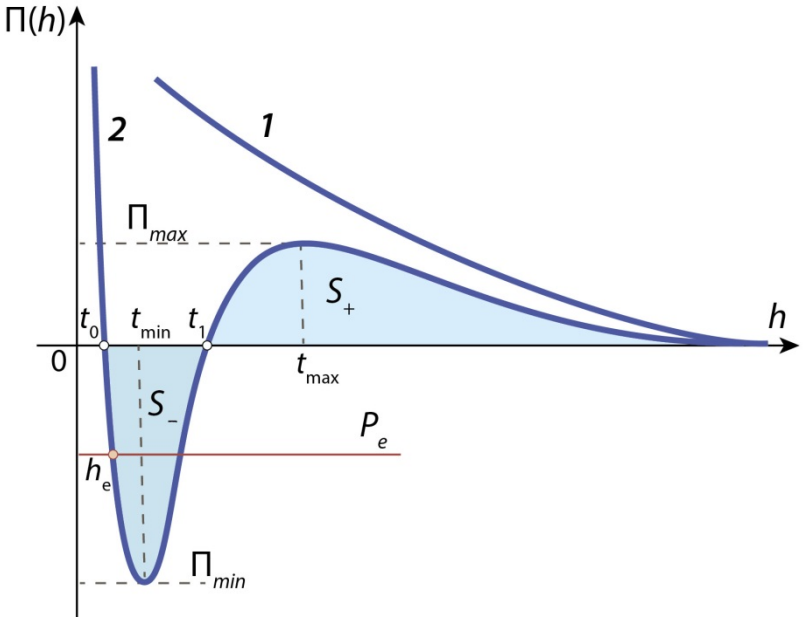

Fig. 2. Disjoining/conjoining pressure isotherms: 1 – complete wetting, 2 – partial wetting. The value h_e defines the equilibrium thickness of equilibrium flat films in the case of drops.

Note, there are two solutions of the equation $\Pi(h_e) = P_e$ at $P_e<0$. However, only one of them satisfies the thermodynamic stability condition $\frac{d\Pi(h_e)}{dh} < 0$ [5].

Static hysteresis of contact angle of sessile droplets on smooth homogeneous substrates

The derivation of Eq. (5) [1,2] shows that it determines a single, unique equilibrium contact angle (at fixed external conditions). Experiments, however, show presence of contact angle hysteresis with an infinite number of apparent "quasi-equilibrium positions" and "quasi-equilibrium contact angles" of a drop on a solid surface: $\theta_r<\theta<\theta_a$, where θ_r and θ_a are static *receding* and *advancing* contact angles. Below "static" is omitted.

Let us consider a liquid drop on a horizontal substrate, which is formed by pumping a fixed volume of the liquid through an orifice in the solid substrate (Fig.3). After pumping is stopped the droplet will form a static advancing contact angle, θ_a. Let us consider the reverse experiment: start pumping the liquid out through the same orifice from the static advancing contact angle, θ_a, which was reached as described above. The contact angle will decrease without the drop base shrinking until a static receding contact angle, θ_r, is reached. After further pumping the liquid out the drop will start receding and eventually will disappear. For water drops on smooth homogeneous glass surfaces, $\theta_r \sim 3^\circ - 10^\circ$, while θ_a is in the range of $40^\circ - 60^\circ$ [2,4].

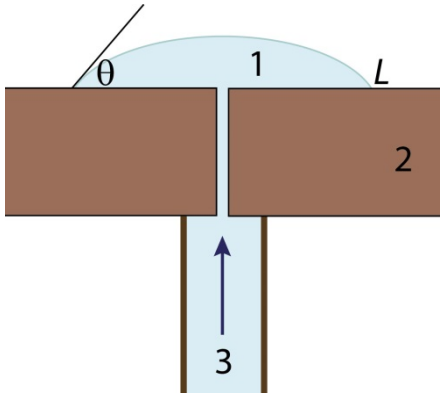

Fig. 3. Schematic illustration of the formation of a drop by appropriate liquid pumping. *L*-radius of the drop base; θ - contact angle. 1- liquid drop, 2- solid substrate with a small orifice in the center, 3 - liquid source/sink (syringe).

Non-equilibrium states of a drop are considered below when the droplet volume is changed by the process described above (see Fig. 3). These states are refereed below as "quasi-equilibrium states". In this case the excess pressure, P, is different from the equilibrium value. As in [1,2] we assume that the main part of the liquid profile is still

described by Eq. (5), where now equilibrium pressure, P_e, should be replaced by a new non-equilibrium pressure, *P:*

$$\frac{\gamma h''}{(1+h'^2)^{3/2}} + \Pi(h) = P\,. \qquad (15)$$

Possible forms of disjoining/conjoining pressure isotherm with a secondary minimum

The disjoining/conjoining pressure is a sum of electrostatic, van der Waals and structural components according to Eq. (4) as it was discussed above.

The structural forces arise due to the orientation of molecules of polar liquid near any interface [5,7]. An example of the structural components calculation according to Eq.(2) is shown in Fig.4.

The parameters K_1, K_2 are pre-exponential factors and the length parameters λ_1, λ_2 are the distances corresponding approximately to a half-decay of the structural forces. The short-range force is usually characterized by value of λ_1 equal to a few nanometers, while the long-range interaction is observed at distances up to 100 nm with values λ_2 = 13-62 nm [7]. For example, in the case of hydrophobic attraction in water between mica surfaces of crossed cylinders hydrophobized by the adsorption layers of fluorocarbon surfactant: λ_1= 2-3 nm, $\lambda_2 \approx$ 16 nm [7].

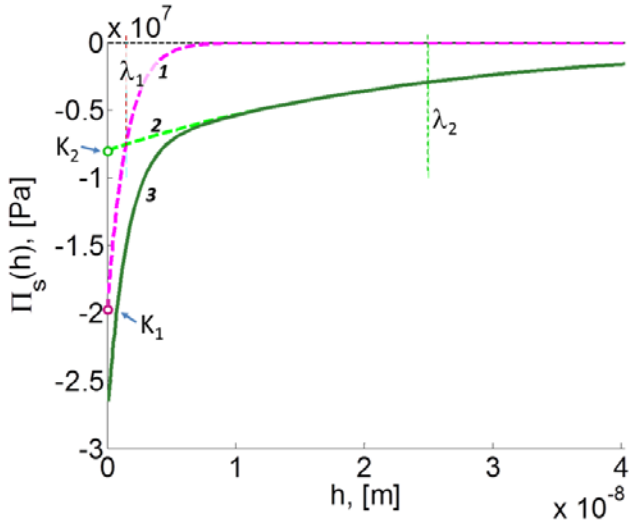

Fig.4. The components of the structural interaction.

1- short-range interaction, $K_1 \exp(-h/\lambda_1)$; 2- long-range interaction, $K_2 \exp(-h/\lambda_2)$; 3 - the total structural interaction, $K_1 \exp(-h/\lambda_1) + K_2 \exp(-h/\lambda_2)$.

K_1 = -2×10^7 Pa; λ_1 = 1.5×10^{-9} m; K_2 = -8×10^6 Pa; λ_2 = 25×10^{-9} m.

In the case of presence of the short-range structural interaction only the disjoining/conjoining pressure isotherms are a sum of the electrostatic, van der Waals and short-ranged structural interactions results in appearance of a single primary minimum (curve 2 in Fig.2). However, the long-range structural forces can cause an additional secondary minimum on the isotherm (see Fig.5). A depth and position of both these minima are determined by parameters of the structural interactions in combination with the parameters of the electrostatic and van der Waals components. The characteristic length of the short-range structural forces, λ_1 is one of the most sensitive parameters; a small variation in λ_1 results in a substantial variation of the form of the disjoining/conjoining pressure isotherms (Fig.5, *a-c*) with various location of the primary and secondary minima. The parameter λ_2 changes the shape of the secondary minimum, but has a weaker influence on the other parts of the isotherm.

An aqueous electrolyte solution of a strong univalent electrolyte has been chosen with the bulk electrolyte concentration c_0 = 1 mole/m^3 and temperature T = 293 °K for calculation of plots in Figs.5,*a-c*. The electrostatic component of the disjoining/conjoining pressure was calculated for the case of constant surface charge density $\sigma_{s,h}$ = const, with values σ_s= -150 mC and σ_h= 150 mC at the boundaries.

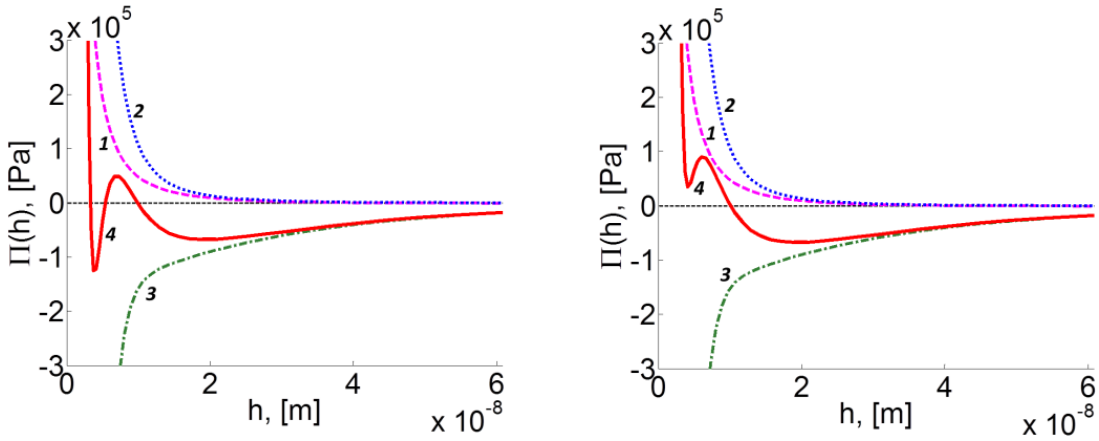

a) *b)*

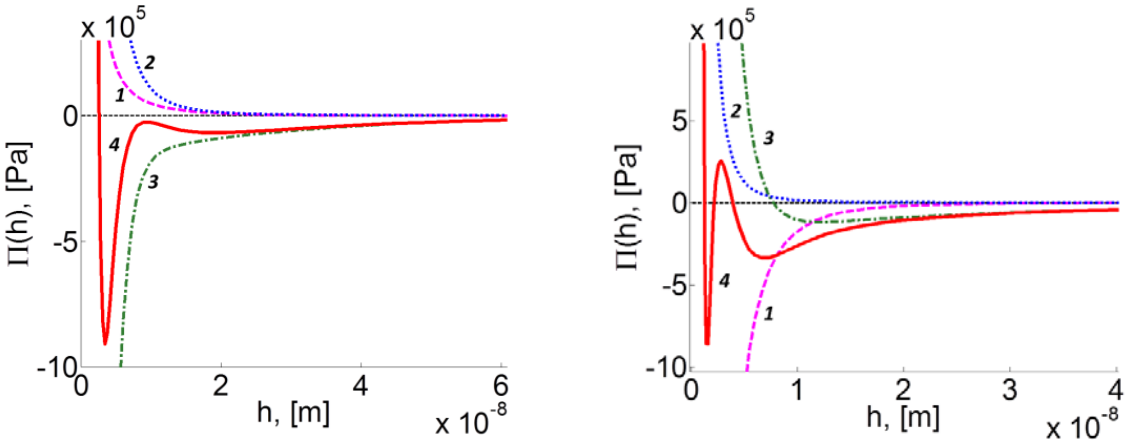

c) *d)*

Fig.5. The disjoining/conjoining pressure isotherms according to Eq (4) for the case of the short-range structural attraction (a-c) ($K_1 < 0$) and repulsion (d) ($K_1 > 0$).

The components of disjoining/conjoining pressure: 1- electrostatic, Π_E; 2 - van der Waals, Π_W; 3 - structural, Π_S; 4 - total interaction, $\Pi = \Pi_E + \Pi_W + \Pi_S$.

Parameters of the electrostatic interaction: constant surface charge of both solid-liquid, σ_s= -150 mC and liquid-vapour, σ_h= -150 mC, interfaces (Figs.5 a, b and c); σ_s= -150 mC; σ_h= 150 mC *(*Fig. 5d*); c_0* = 1 mole/m^3, *T* = 293 K. Parameters of the van der Waals and structural interactions: *A* = 2×10^{-18} J*;* K_1 = -3.7×10^7 Pa; K_2 = -2×10^5 Pa; λ_2 = 25×10^{-9} m.

a) λ_1 = 1.35×10^{-9} m; *b)* 1.31×10^{-9}; *c)* 1.5×10^{-9};

d) K_1 = 3×10^7 Pa; K_2 = -2×10^5 Pa; λ_1 = 1.45×10^{-9} m; λ_2 = 25×10^{-9} m.

In the case of the short-range structural repulsion, the parameter K_1 in Eq.(2) is positive and the structural forces change a sign depending on the distance: they are repulsive or attractive at different distances. Now the disjoining/conjoining pressure isotherms can include two minima (Fig.5) separated by a barrier.

Thus, the disjoining/conjoining pressure isotherms with two minima are possible if the structural interactions are included with both short-ranged and long-ranged parts acting at different distances: the long-range interaction is always attractive; the short-range one can be either attractive or repulsive.

Expressions for the advancing contact angle

Advancing contact angles are formed at $P < P_e$. The condition for the existence of a solution of Eq. (15) is written for a quasi-equilibrium drop in the following form (identical to (10)):

$$\gamma \geq \varphi(h, P) \geq 0\,, \qquad (16)$$

where now the function $\varphi(h, P)$ is given by:

$$\varphi(h, P) = -P(H - h) + \int_h^\infty \Pi(h)dh\,. \qquad (17)$$

In Fig. 6 examples of dependences $\varphi(h, P)$ (Fig. 6, curves *2-3)* for the disjoining/conjoining pressure isotherm $\Pi(h)$ (Fig.6, curve 1) are presented. The max/min of $\varphi(h, P)$ are found from the condition $P = \Pi(h)$, in the same way as in the case of equilibrium, i.e., from the points of intersection of the disjoining/conjoining pressure isotherm with the straight line $P = const$. It follows from Eq. (17) that in the case of equilibrium drop, i.e., at $P = P_e$, the function $\varphi(h, P_e)$ vanishes at both $h = h_e$ and $h = H$. Since $\varphi(h, P_e) > 0$, the function $\varphi(h, P_e)$ has a maximum at $h = h_2$ (Fig. 6, curve 2).

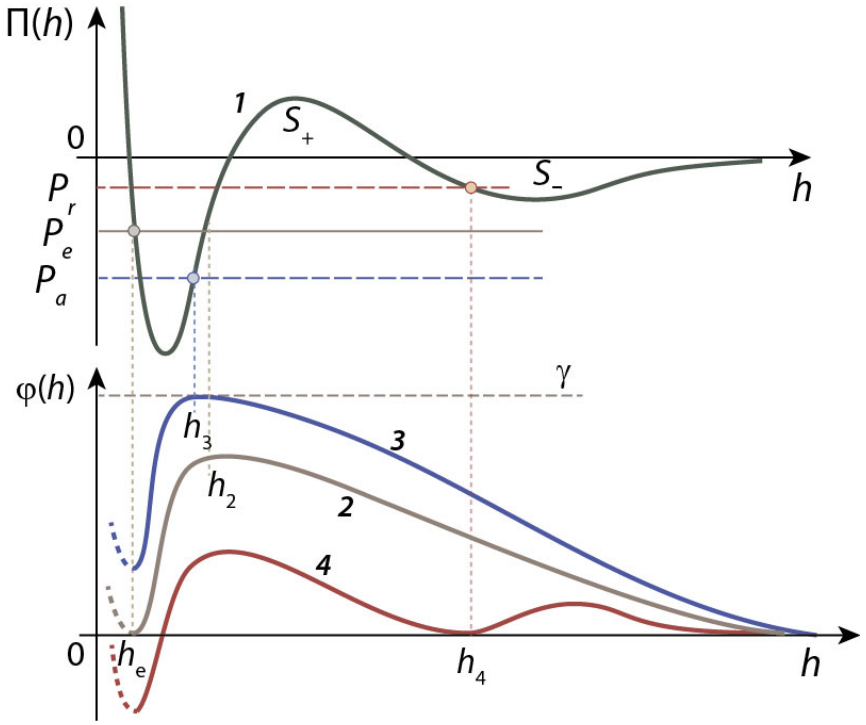

Fig. 6. Disjoining/conjoining pressure isotherm $\Pi(h)$, upper part: the case of *partial* wetting (curve 1); lower part: functions $\varphi(h, P)$ (17). At equilibrium, $\varphi(h, P_e)$ (curve 2), and quasi-equilibrium, $\varphi(h, P)$, before the advancing (curve 3) and receding (curve 4) starts.

At lower pressures, that is at $P < P_e$, the drop surface becomes more convex than at equilibrium, the line $\varphi(h, P)$ (Figure 6, curve 3) is located above the equilibrium curve 2 (Fig. 6). The condition of quasi-equilibrium is violated and the perimeter of the drop starts to advance after the maximum of $\varphi(h, P)$ reaches the dashed line $\gamma = const$ (curve 3, Fig. 6). This condition corresponds to the appearance of a thickness with a vertical tangent $h' = \infty$ on the profile of the drop. After that the liquid will flow from the drop on to the film in front by the so-called Frenkel's "caterpillar" mechanism at further decrease of P, when $\varphi(h, P) > \gamma$. This shows that the static *advancing* contact angle does not depend on the roughness of the solid substrate if size of roughness is below the value of h_3~10-30 nm (Fig. 6, curve 3), a phenomenon well known experimentally [27]. The values of h_3 is found below from the shape of disjoining/conjoining pressure isotherm (see e.g. Figs. 5, 7). The point h_3 was found to be located very close to the primary minimum at $h > h_{min}$, so the values h_3~10-30 nm correspond approximately to the primary minimum.

Let us calculate the value of the *advancing* contact angle θ_a, using the condition $\varphi(h_3, P) = \gamma$:

$$-P_a(H_a - h_3) + \int_{h_3}^{\infty} \Pi(h) dh = \gamma \,. \qquad (18)$$

Note, the droplet volume according to the procedure described above is fixed, V_a.

Keeping in mind that $P_a = \gamma (\cos \theta_a - 1)/H_a$, it is possible to conclude using Eq. (18) that

$$\cos\theta_a = \frac{P_a h_3}{\gamma} + \frac{1}{\gamma}\int_{h_3}^{\infty} \Pi(h) dh \approx \frac{1}{\gamma}\int_{h_3}^{\infty} \Pi(h) dh \,. \qquad (19)$$

Let us calculate the difference $\cos\theta_e - \cos\theta_a$ using Eq. (13) for the equilibrium contact angle, θ_e, equilibrium excess pressure, P_e, in the drop, and Eq. (19). We obtain

$$\cos\theta_e - \cos\theta_a = 1 + \frac{1}{\gamma}\int_{h_e}^{h_3} \Pi(h) dh > 0 \,. \qquad (20)$$

In the case of partial wetting $\theta_e < 90°$ and $\cos\theta_e > 0$, hence, the integral $\frac{1}{\gamma}\int_{h_e}^{\infty} \Pi dh < 0$ from Eq.(13) and the absolute value of the integral does not exceed 1. Therefore, $\left|\frac{1}{\gamma}\int_{h_e}^{h_3} \Pi dh\right| < 1$. Hence, $\cos\theta_e - \cos\theta_a > 0$ and $\theta_a > \theta_e$ according to Eq.(20). Thus *advancing* contact angle is always bigger than the *equilibrium* contact angle in agreement with experimental observations.

If we assume that the disjoining/conjoining pressure isotherm changes very abruptly between t_{min} and t_1 (Fig. 2 and Fig. 6, upper part), then $h_3 \approx t_{\min} \approx t_1 = const$. In this case Eq. (19) results in

$$\cos\theta_a = \frac{S_+ - S_=}{\gamma}. \qquad (21)$$

The *advancing* contact angle according to the developed above theory is determined below according to the following procedure. P_a is determined from equation $P_a = \Pi(h_3)$ as a function of the thickness h_3. However, the equation $P_a = \Pi(h_3)$ has two roots. The second root, not the first one of the latter equation should be selected (Fig. 6, curve 3). According to Eq. (18) this yields: $-\Pi(h_3)(H_a - h_3) + \int_{h_3}^{\infty} \Pi(h)dh = \gamma$, that provides the unknown height of the drop H_a as a function of h_3:

$$H_a = h_3 + \frac{\gamma - \int_{h_3}^{\infty} \Pi(h)dh}{-\Pi(h_3)}, \qquad (22)$$

where $P_a = \Pi(h_3) < 0$ and $\gamma - \int_{h_3}^{\infty} \Pi(h)dh > 0$.

Let R_a be the radius of curvature of the drop at the moment of advancing. A simple geometrical consideration shows that

$$L_a = R_a \sin\theta_a = -\frac{\gamma \sin\theta_a}{\Pi(h_3)}, \qquad (23)$$

where L_a is the radius of the droplet base at the moment when advancing contact angle is reached.

The volume of the two-dimensional drop at the moment of advancing, V_a, can be expressed as

$$V_a = \frac{L_a^2}{\sin^2\theta_a}(\theta_a - \sin\theta_a \cos\theta_a). \qquad (24)$$

From Eq. (24) we conclude:

$$L_a = \sin\theta_a \sqrt{\frac{V_a}{(\theta_a - \sin\theta_a \cos\theta_a)}}. \qquad (25)$$

Combination of Eqs. (23) and (25) results in

$$\sqrt{\frac{V_a}{\left(\theta_a - \sin\theta_a \cos\theta_a\right)}} = -\frac{\gamma}{\Pi(h_3)}, \qquad (26)$$

where the contact angle θ_a is expressed as

$$\cos\,\theta_a = \frac{\Pi(h_3)h_3}{\gamma} + \frac{1}{\gamma}\int_{h_3}^{\infty} \Pi dh \qquad (27)$$

and $\sin\,\theta_a = \sqrt{1-\cos^2\,\theta_a}$.

The values h_3 and θ_a as functions of the droplet volume, V_a, are found by solving Eqs.(26)-(27). Thus, the developed theory predicts a dependency of the advancing contact angle on the droplet volume V_a.

The dependency of the advancing contact angle on the droplet volume was directly confirmed experimentally in [21-22]. In [21] the author showed that the advancing contact angle of droplets really increases as the volume of the droplet decreases. In [22] the advancing contact angle of bubbles was considered and the authors arrived to the same conclusion. Such result was predictable as the equilibrium contact angle according to Eq. (13) is also a function of the droplet volume. Hence, that static *advancing* contact angle in the case of drops is not a unique characteristic of solid substrates but determined also by the droplet volume.

Expressions for the receding contact angle

If the disjoining/conjoining pressure isotherm includes the structural component, two additional points of intersection are possible of $\Pi(h)$ with *P=const* (Fig.6, curve 1). In this case the expressions for the receding contact angle can be obtained in a similar as above for the case of advancing contact angle.

At higher pressures, i.e., for $P > P_e$ (the liquid is pumped out from the droplet, the arrow in Fig. 3 should be directed downward). The droplet surface becomes less convex, the line $\varphi(h, P)$ (Fig. 6, curve 4) is located below the equilibrium curve 2 (Fig. 6). The condition of quasi-equilibrium is violated and the perimeter of the drop starts to recede after the minimum of $\varphi(h, P)$ reaches zero (curve 4, Fig. 6). This condition corresponds to the appearance of a thickness with a horizontal tangent $h' = 0$ on the profile of the drop. After that the droplet starts to slide over thick β – film.

The expressions for the receding contact angle can be determined from the condition $\varphi(h, P)=0$:

$$P_r(H_r - h_4) - \int_{h_4}^{\infty} \Pi dh = 0 \tag{28}$$

From Eq.(28) the droplet height at the moment of receding is

$$H_r = h_4 + \frac{1}{P_r}\int_{h_4}^{\infty} \Pi dh. \tag{29}$$

For the two dimensional spherical droplet:

$$P_r = \gamma\,(\cos\theta_r - 1)/H_r. \tag{30}$$

The receding contact angle is expressed from Eqs. (30) and (28) as

$$\cos\theta_r = 1 + \frac{P_r H_r}{\gamma} = 1 + \frac{P_r h_4}{\gamma} + \frac{1}{\gamma}\int_{h_4}^{\infty} \Pi dh. \tag{31}$$

It is assumed that the droplet base does not shrink during the transition between the advancing and receding contact angles, i.e. L_a=L_r=const, which is in accordance with numerous experimental observations.

Then the radius of the base of the contact line, $L_r = R_r \sin\theta_r$, is expressed using Eq.(31) as

$$L_r = -\frac{\gamma}{\Pi(h_4)}\sqrt{1 - \left(1 + \frac{\Pi(h_4)h_4}{\gamma} + \frac{1}{\gamma}\int_{h_4}^{\infty} \Pi dh\right)^2} = L_a. \tag{32}$$

The value h_4 is found from Eq.(32), where L_a is already known from Eq. (25). The drop volume at the moment of receding is as follows:

$$V_r = \frac{L_a^2}{\sin^2\theta_r}\left(\theta_r - \sin\theta_r\cos\theta_r\right). \tag{33}$$

The following algorithm of calculation of dependence of the advancing and receding contact angles on the droplet volume was used below:

1. A particular disjoining/conjoining pressure isotherm and the value V_a are selected.

2. The system of Eqs (26)-(27) is solved; the values h_3 and θ_a are determined.

3. The droplet base radius L_a for the advancing case is calculated according to Eq (25).

4. Using the obtained value L_a, the value h_4 is found from Eq.(32) for the receding case.

5. The droplet heights H_a and H_r are calculated using Eqs (22) and (29).

6. The advancing and receding contact angles are found from Eqs.(27) and (31).

7. The function $\varphi(h, P)$ for the both cases is plotted using Eq (17).

8. The receding volume, V_r , is calculated according to Eq.(33).

9. The droplet profiles are calculated by integration of Eq.(5).

The calculated results are presented in Fig.7, which show that $\theta_r < \theta_a$ as expected. During the transition from the advancing to receding state, the droplet volume decreases due to pumping out the liquid, hence, $V_r < V_a$. The absolute value of the excess pressure decreases also, $|P_r| < |P_a|$; the droplet is getting 'flatter', i.e. the radius of curvature, $R_r = -\gamma/P_r$, grows (Fig.7).

The obtained simulation results are: advancing contact angle ~ 57°, while the receding contact angle is ~ 8°, which agree with experimental data [2,4]. Note, the disjoining/conjoining pressure isotherm used for these calculations is selected similar to that known for glass surfaces [4].

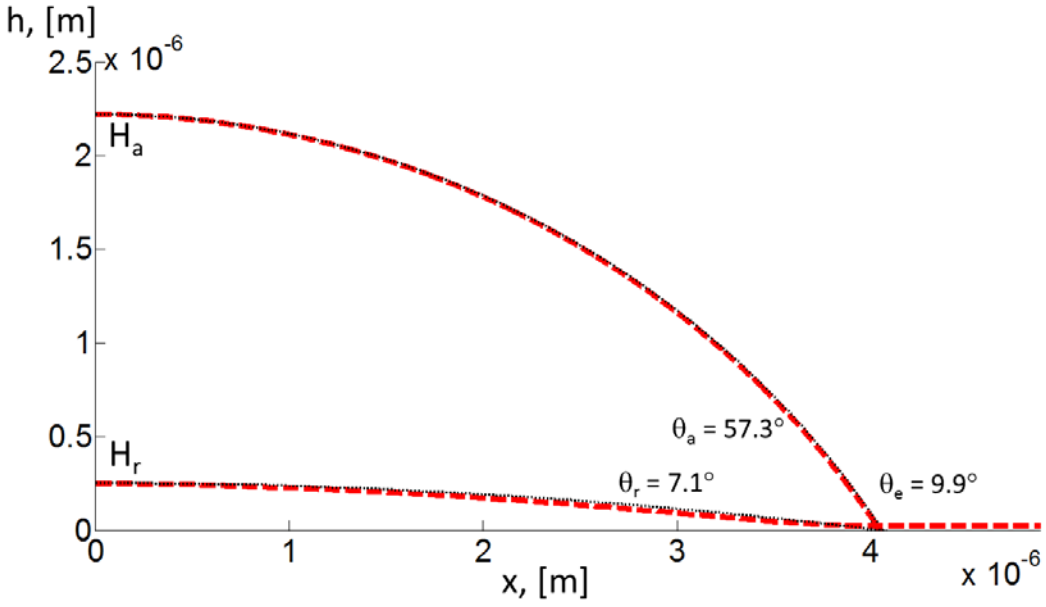

Fig.7. The droplet profiles at advancing and receding contact angles.

Advancing: $V_a = 1.0\times10^{-11}$ m^3; θ_a= 57.3°; $P_a = -2.05\times10^4$ Pa; $H_a = 2.2\times10^{-6}$ m;
Receding: $V_r = 7.58\times10^{-13}$ m^2; θ_r= 7.1°; $P_r = -3.09\times10^3$ Pa; $H_r = 2.5\times10^{-7}$ m.

The parameters of the disjoining/conjoining pressure isotherm: σ_s= -150 mC; σ_h= 120 mC; c_0 =1×10^{-2} mole/m^3; $A = 3.5\times10^{-20}$ J; $K_1 = 2.0\times10^7$ Pa; $K_2 = -1\times10^4$ Pa; $\lambda_1 = 3.6\times10^{-9}$ m; $\lambda_2 = 26\times10^{-9}$ m.

The effect of variation of the drop volume, V_a, on the hysteresis contact angles is presented in Fig.8. The higher the initial volume of the droplet V_a the lower the values of both θ_a and θ_r are (Fig. 8a). The highest values of the hysteresis contact angles are found for small drops with a high excess pressure, γ/R. This relation between the contact angle and the droplet volume agrees with experimental data [21, 22].

A final (receding) size of the droplet depends on the initial volume of the droplet. Almost linear dependence between the volumes V_r and V_a was obtained (Fig. 8b): the bigger the initial droplet, the bigger the final one.

Let us write down for comparison the expressions for the advancing, equilibrium and receding contact angles:

$$\cos\theta_a = \frac{\Pi(h_3)h_3}{\gamma} + \frac{1}{\gamma}\int_{h_3}^{\infty}\Pi dh \tag{34}$$

$$\cos\theta_e = 1 + \frac{1}{\gamma}\int_{h_e}^{\infty}\Pi dh \tag{35}$$

$$\cos\theta_r = 1 + \frac{\Pi(h_4)h_4}{\gamma} + \frac{1}{\gamma}\int_{h_4}^{\infty}\Pi dh \tag{36}$$

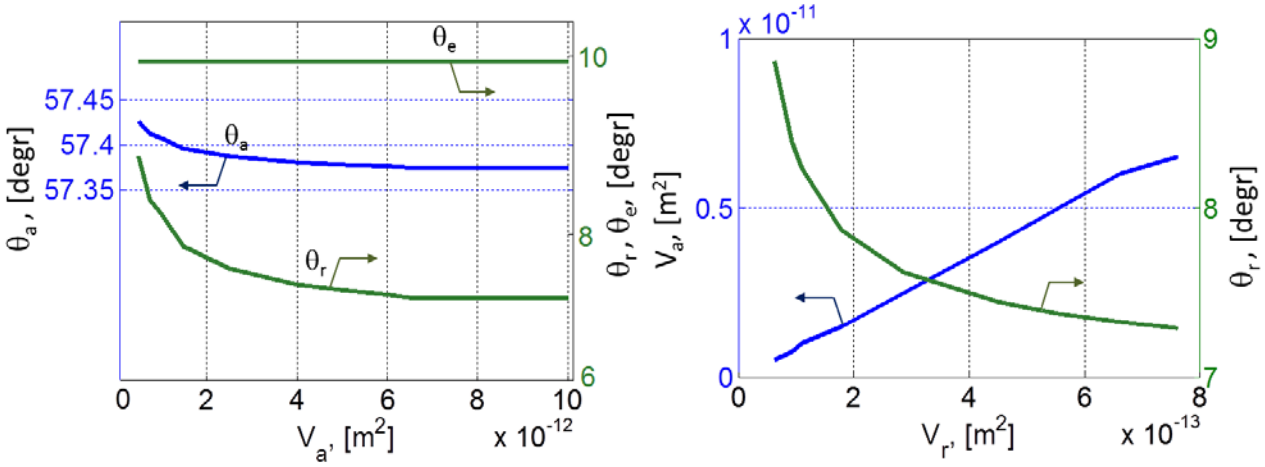

a b

Fig.8. The relations between the values θ_a, θ_r, θ_e, V_a and V_r (data from Fig.7 at variation of V_a). Note the different scales for the left and right vertical axes.

As it was mentioned above equilibrium droplets can exist at oversaturation only and the oversaturation determines the droplet volume, which ion its turn determines L_e. However, we made selection just the in the opposite way: we selected L_e=L_a and determine the required oversaturation pressure *p* according to Eq.(6). The equilibrium values of the contact angle θ_e were calculated from the condition using Eq.(35). Eq.(6) and equation for the droplet height *H* below Eq.(14) are satisfied for equilibrium droplets.

As was mentioned above the values of the equilibrium contact angle are located between the values for advancing and receding cases: $\theta_r < \theta_e < \theta_a$. The calculation results agree with this conclusion (Fig. 8a). The calculations demonstrate also that the equilibrium contact angle practically does not depend on the droplet volume. A reason for this behavior can be understood from the shape of the disjoining/conjoining pressure isotherm (see e.g. Fig. 6): the value h_e (corresponding to a point of intersection between $\Pi(h)$ and P_e) changes very slightly at variations of P_e. This is because $\Pi(h)$ changes very abruptly at low h. Hence, according to Eq. (35), there is a very weak dependence of the equilibrium contact angle, θ_e, on P_e and, consequently, θ_e on the droplet volume.

As follows from data presented in Fig. 8a, the values θ_e are much closer to θ_r than to θ_a, i.e. θ_e-θ_r << θ_a-θ_e.

The experimental data presented in [23-24] showed that the hysteresis effect in the case of smooth homogeneous surfaces is not related to roughness or chemical

heterogeneity of the substrate. It was concluded in [23-24] that the hysteresis phenomenon can be explained within the framework of the theory [25] which was developed earlier using a similar approach for some particular cases of the disjoining/conjoining pressure isotherms.

Note, the evaporation, which takes place more intensively in vicinity of the three-phase contact line [26], makes the measurements of both advancing and receding contact angles of drops not so straightforward and unambiguous in the case of volatile liquids. It is the reason why a number of experiments on wetting/spreading of liquids have been performed in thin capillaries, where evaporation can be significantly diminished if not ruled out 923, 24].

Conclusions

Based on the developed theory the contact angle hysteresis on smooth, homogeneous solid substrates in terms of the disjoining/conjoining pressure was theoretically investigated. It was shown that for any value of the contact angle, θ, from the range $\theta_r < \theta < \theta_a$, except the equilibrium value $\theta = \theta_e$, a slow "microscopic" advancing or receding motion of the liquid takes place in a vicinity of the apparent three phase contact line.

Expressions for advancing/receding contact angles of droplets on smooth homogeneous solid substrates deduced via isotherm of disjoining/conjoining pressure. It was shown that both advancing and receding contact angles of a droplet on a smooth homogeneous solid substrate depend on the drop volume and are not a unique characteristic of the liquid-solid system. It was shown also that the receding contact angle is much close to equilibrium contact angle. The latter conclusion is in contradiction with commonly accepted view that the advancing contact angle can be taken as the first approximation for equilibrium contact angle. The suggested mechanism of contact angle hysteresis of contact angle of droplets has a direct experimental confirmation.

Acknowledgement

This work was supported by CoWet ITN, EU; Engineering and Physical Sciences Research Council, UK, grant EP/D077869/1; ESA under grant PASTA; COST MP1106 project; and UK-Russia joint project, the Royal Society, UK.

References

(1) Starov, V.M.; Velarde, M.G. Surface forces and wetting phenomena. *J. Phys.: Condens. Matter*, 21, **2009**, 464121 (11pp).

(2) Starov, V.; Velarde, M.; Radke, C. *Wetting and Spreading Dynamics*. In "Surfactant Science Series", v. 138, Taylor&Francis, **2007**, 515 pp.

(3) Churaev, N. V.; Sobolev, V. D.; Starov, V.M. Disjoining Pressure of Thin Nonfreezing Interlayers. *J Colloid Interface Sci*, **2002**, 247**,** 80–83.

(4) Churaev, N.V.; Sobolev, V.D. Prediction of contact angles on the basis of the Frumkin-Derjaguin approach. *Adv Colloid Interface Sci*, **1995***,* 61, 1-16*.*

(5) Derjaguin, B.V.; Churaev, N.V.; Muller, V.M. *Surface Forces,* Springer, 1987.

(6) Kuchin, I.V.; Matar, O.K.; Craster, R.V.; Starov, V.M. Influence of the disjoining pressure on the equilibrium interfacial profile in transition zone between a thin film and a capillary meniscus. *Colloid and Interface Science Communications*, **2014**, 1, 18-22.

(7) Churaev, N.V.; Sobolev, V.D. Wetting of low energy surfaces. *Adv. Colloid Interf. Sci.*, **2007**, 134–135, 15–23.

(8) Starov, V. Static contact angle hysteresis on smooth, homogeneous solid substrates. *Colloid Polym Sci*, **2013**, 291:261–270.

(9) Chibowski, E. Surface free energy of a solid from contact angle hysteresis. *Adv. Colloid Interface Sci*., **2003**, 103**,** 149–172.

(10) Extrand, C. W.; Kumagai, Y. An experimental study of contact angle hysteresis. *J. Colloid Interface Sci.,* **1997**, 191**,** 378–383.

(11) Extrand, C. W. Water contact angle and hysteresis of polyamid surfaces. *J. Colloid Interface Sci.,* **2002**, 248**,** 136–142.

(12) Zorin, Z.M.; Sobolev, V.D.; Churaev, N.V. *Surface Forces in Thin Films and Disperse Systems*, **1972**, Nauka, Moscow, p. 214. [in Russian]

(13) Romanov, E.A.; Kokorev, D.T.; Churaev, N.V. Effect of wetting hysteresis on state of gas trapped by liquid in a capillary. *Int. J. Heat Mass Transfer*, **1973**, 16, 549-554.

(14) Rangelova, N.; Platikanov, D. *Annals Univ. Sofia, Fac.Chim.,* **1976/1977**, 71/72**,** 109;

(15) Platikanov, D.; Yampolskaya, G.P.; Rangelova, N.; Angarska, Zh.; Bobrova, L.E.; Izmailova, V.N. Free black films of proteins. Thermodynamic parameters. *Colloid J.,* USSR, **1981**, 43**,** 177-180.

(16) Rangelova, N.; Platikanov, D. *Annals Univ. Sofia, Fac. Chim.,* **1984**, 78**,** 126.

(17) Rangelova, N.I.; Izmailova, V.N.; Platikanov, D.N.; Yampol'skaya, G.P.; Tulovskaya, S.D. Free black films of proteins: dynamic hysteresis of the contact angle (film-bulk liquid) and the rheological properties of adsorption layers. *Colloid J.,* USSR, **1990**, 52, 442-447.

(18) Platikanov, D.; Nedyalkov, M.; Petkova, V. Phospholipid black foam films: dynamic contact angles and gas permeability of DMPC bilayer films. *Adv. Colloid Interface Sci.,* **2003**, 101-102, 185-203.

(19) Petkova, V.; Platikanov, D.; Nedyalkov, M. Phospholipid black foam films: dynamic contact angles and gas permeability of DMPC+DMPG black films. *Adv. Colloid Interface Sci.,* **2003**, 104**,** 37-51.

(20) Sagan, H. *Introduction to the Calculus of Variations*. Dover reprint, New York, **1992**, chapter 7.

(21) Mack, G. L. The Determination of Contact Angles from Measurements of the Dimensions of Small Bubbles and Drops. I. The Spheroidal Segment Method for Acute Angles. *J Phys Chem.,* **1936**, 40 (2), 159-167.

(22) Veselovsky, V.S.; Pertsev, V.N. Adhesion of the bubbles to solid surfaces. *J. Phys Chem (USSR Academy of Sciences),* **1936**, 8 (2), 245-259 (in Russian).

(23) Zorin, Z. M.; Romanov V. P.; Churaev, N. V. Effect of surfactants on wetting of quartz by electrolyte solutions. *Kolloidn. Zh.*, **1979**, 41(6), 1066-1073.

(24) Zorin, Z. M.; Romanov, V. P.; Churaev, N. V. The contact angles of surfactant solution on the quartz surface. *Colloid & Polymer Sci.*, **1979**, 257, 968-972.

(25) Martynov, G. A.; Starov, V. M.; Churaev, N. V. Hysteresis of the contact angle on homogeneous surfaces. *Kolloidn. Zh.*, **1977**, 39, 472-484.

(26) Semenov, S.; Trybala, A.; Rubio, R.G.; Kovalchuk, N.; Starov, V.; Velarde, M.G. Simultaneous spreading and evaporation: Recent developments. *Adv Colloid Interface Sci,* **2014**, 206, 382–398.

(27) Johnson, R.E., Dettre, R.H. Contact angle, wettability and adhesion. *Adv. Chem. Ser.,* **1964**, 43, 112–135.

Table of Contents/Abstract Graphic